Front. Mater. Sci. 2020, 14(2): 109–119
https://doi.org/10.1007/s11706-020-0497-5

RESEARCH ARTICLE

Two-step preparation of carbon nanotubes/RuO_2/polyindole ternary nanocomposites and their application as high-performance supercapacitors

Danhua ZHU[1*], Qianjie ZHOU[1*], Aiqin LIANG[1], Weiqiang ZHOU (✉)[1], Yanan CHANG[1], Danqin LI[1], Jing WU[1], Guo YE[1], Jingkun XU (✉)[1], and Yong REN[2]

1 Jiangxi Key Laboratory of Organic Chemistry, Jiangxi Science and Technology Normal University, Nanchang 330013, China
2 Department of Mathematical Sciences, Zibo Normal College, Zibo 255130, China

ABSTRACT: A ternary single-walled carbon nanotubes/RuO_2/polyindole (SWCNT/RuO_2/PIn) nanocomposite was fabricated by the oxidation polymerization of indole on the prefabricated SWCNT/RuO_2 binary nanocomposites. The nanocomposite was measured by FTIR, XRD, SEM, TEM, EDS and XPS, together with the electrochemical technique. The electrochemical results demonstrated that the symmetric supercapacitor used SWCNT/RuO_2/PIn as electrodes presented 95% retention rate after 10000 cycles, superior capacitive performance of 1203 $F \cdot g^{-1}$ at 1 $A \cdot g^{-1}$, and high energy density of 33 $W \cdot h \cdot kg^{-1}$ at 5000 $W \cdot kg^{-1}$. The high capacitance performance of SWCNT/RuO_2/PIn nanocomposite was mainly ascribed to the beneficial cooperation effect among components. This indicated that the SWCNT/RuO_2/PIn nanocomposite would be a good candidate for high-performance supercapacitors.

KEYWORDS: SWCNT/RuO_2/PIn; nanocomposite; supercapacitor

Contents

Received December 6, 2019; accepted February 6, 2020

E-mails: zhouwqh@163.com (W.Z.), xujingkun@tsinghua.org.cn (J.X.)

* D.Z. and Q.Z. contributed equally to this work.

1 Introduction

Supercapacitors (SCs), as environmentally friendly green energy, are deemed as one of the most popular energy storage systems due to the high power density, very fast charging/discharging time, along with excellent cycling life [1–2]. Depending on the energy storage mechanism, SCs are subdivided in two categories: electric double-layer capacitors (EDLCs), where charge accumulates at the interface of electrode and electrolyte, and pseudocapacitors that the active materials emerge reversible redox reactions [3–4]. For EDLCs, carbon materials including activated carbons [5], carbon nanotubes (CNTs) [6], carbon

nanofibers (CNFs) [7], graphene (GE) [8], etc. have been widely utilized as electrode materials because of their good electrical conductivity and satisfactory stability [9], however, they are embodied low specific capacitance and energy density. Pseudocapacitors employ metal oxides (e.g., RuO_2 and MnO_2) and conducting polymers (CPs) including polyaniline (PAN), polypyrrole (PPy) and poly (3,4-ethylenedioxythiophene) (PEDOT) as active electrode materials [10–11]. Although they have high specific capacitance, their poor stability and small power density become weakness. For the development of supercapacitor electrodes, one strategy is to construct various nanocomposites, and there have been a few reports about ternary nanocomposites such as MnO_2/CNT/PEDOT-PSS (427 $F \cdot g^{-1}$) [12], MnO_2/CNT/PEDOT (481 $F \cdot g^{-1}$) [13], MnO_2/PPy/CNF (705 $F \cdot g^{-1}$) [14], CNT/PPy/MnO_2 (325 $F \cdot g^{-1}$) [15], and CNT/PAN/MnO_2 (330 $F \cdot g^{-1}$) [16].

Among CPs, polyindole (PIn) has been found to be one of promising electroactive materials due to its relatively high thermal stability and excellent redox activity. In addition, the electrochemical stability of PIn is better than those of PAN and PPy [17–18]. However, the low conductivity of PIn limits its application in supercapacitors [19]. In order to arise the capacitance performance of PIn, several PIn composites have been reported, such as PIn/CNT [20–21], CNT/PIn/GE [22], PEDOT:PSS/PIn [23], RGO/PIn [18], PIn/carbon black/MoS_2 [24], V_2O_5/PIn/carbon cloth [25] and Co_3O_4@MWCNTs/PIn [26]. Among those composites, the metal oxides (e.g., V_2O_5 and Co_3O_4) could markedly increase the capacitance. For instance, the specific capacitances of Co_3O_4@MWCNTs/PIn in PVA/NaOH gel electrolytes and V_2O_5/PIn/carbon cloth composite in 5 $mol \cdot L^{-1}$ $LiNO_3$ aqueous solution reached 442.5 and 535.3 $F \cdot g^{-1}$, respectively [25–26]. The Co_3O_4/PIn composites prepared by *in-situ* cathodic electrodeposition exhibited an exceptional values as high as 1805 $F \cdot g^{-1}$ in 1 $mol \cdot L^{-1}$ KOH solution [27]. However, we know that PIn can show marvelous redox activity in acidic electrolyte, whereas its electrochemical activity is very poor in basic solution and neutral aqueous solution. Therefore, in terms of the beneficial synergistic effects, there are shortcomings for the construction of Co_3O_4/PIn and V_2O_5/PIn composites because of sacrificing the excellent electrochemical activity of PIn. So it is very significant to rationally design a composite material by incorporating metal oxide with high electrochemical behaviors in acidic aqueous solution into PIn, which will maximize the synergistic effects between metal oxide and PIn.

Ruthenium oxide (RuO_2) has high theoretical specific capacitance, good conductivity as well as rapid charging/discharging features in acidic aqueous solution [28–29]. Although the high cost of RuO_2 is deemed as a restrictive factor for its application, recently, RuO_2-based nanocomposites have received renewed attention for their potential application in supercapacitors [30] such as RuO_2/GE (570 $F \cdot g^{-1}$) [31], RuO_2/GE/CNT (502 $F \cdot g^{-1}$) [32], RuO_2/PEDOT:PSS/GE (820 $F \cdot g^{-1}$) [33]. However, metal oxides tend to suffer from low cycling and mechanical stability due to the dissolution occurs during the electrochemical redox reaction [34]. To overcome these drawbacks, in this work, a ternary nanocomposite of SWCNT/RuO_2/PIn was firstly prepared through a simple *in situ* oxidation polymerization of indole on SWCNT/RuO_2. In this ternary nanocomposite, SWCNT effectively avoided the agglomeration of RuO_2 nanoparticles, prominently enhanced the electronic conductivity, and the outmost PIn layer was proven to further enhance the specific capacitance and stability of SWCNT/RuO_2 nanoparticles. As was expected, the SWCNT/RuO_2/PIn nanocomposite showed superhigh specific capacitance of 1307 $F \cdot g^{-1}$ at 0.5 $A \cdot g^{-1}$, good rate capability together with long cycling life. Furthermore, the symmetric supercapacitor based on SWCNT/RuO_2/PIn electrodes was also valuated in detail.

2 Experimental

2.1 Materials

SWCNT aqueous dispersion was purchased from Nanjing XFNANO Materials Tech Co., Ltd.). Ruthenium(III) chloride hydrate ($RuCl_3 \cdot nH_2O$) came from Sinopharm Chemical Reagent Co., Ltd. Indole (99% purity), ammonium peroxodisulfate (APS), sodium hydroxide (NaOH), ethanol were purchased from Shanghai Vita Chemical Reagent Co., Ltd. The concentrated H_2SO_4 was bought from Jinan Chemical Reagant Co.

2.2 Preparation of SWCNT/PIn and SWCNT/RuO_2

The SWCNT/PIn nanocomposite was synthesized via an oxidation polymerization method of indole in the presence of SWCNT and APS, in which the mass ratio of SWCNT to indole was 1:11.7. Namely, 0.2 $mol \cdot L^{-1}$ APS solution was added dropwise into indole (0.1 $mol \cdot L^{-1}$) ethanol solution containing SWCNT. After 12 h, the products obtained by filter were washed repeatedly with deionized water and

ethanol, subsequently dried under vacuum at 60 °C for 24 h, and finally the SWCNT/PIn nanocomposite was obtained.

To make the SWCNT/RuO_2 nanocomposite, a solution of 0.01 mol·L^{-1} ruthenium chloride aqueous solution containing SWCNT (the mass ratio of SWCNT to ruthenium chloride was 1:8.3) was stirred for 30 min. Subsequently, 1.0 mol·L^{-1} NaOH solution was used to tune the pH to 7. After reaction for 6 h, the sediment was filtered, washed, and dried at 60 °C under vacuum and then at 180 °C for 2 h, thus obtaining the SWCNT/RuO_2 nanocomposite.

2.3 Preparation of SWCNT/RuO_2/PIn

To make the ternary composite, 0.1 mol·L^{-1} indole ethanol solution containing aforementioned SWCNT/RuO_2 (the mass ratio of SWCNT/RuO_2 to indole was 1:6.7) was ultrasonicated for 30 min, subsequently added 0.2 mol·L^{-1} APS solution. After 12 h, the sediment was filtered, washed, and dried under vacuum at 60 °C, thus gaining the SWCNT/RuO_2/PIn nanocomposite.

2.4 Characterization

Scanning electron microscopy (SEM) and transmission electron microscopy (TEM) were carried out on Hitachi-S4800 scanning electron microscope and FEI TECNAI G2 F20 microscope at an acceleration voltage of 200 kV, respectively. X-ray photoelectron spectroscopy (XPS) was carried out on an X-ray photoelectron spectrometer (K-Alpha, USA) with Al Kα X-ray radiation as the X-ray source for excitation. The D8 Advance instrument and the Bruker Vertex 70 Fourier transform infrared spectrometer were respectively used to obtain X-ray diffraction (XRD) and Fourier transform infrared spectroscopy (FTIR) data of samples. Electrochemical tests were performed using CHI 660E instrument. The electrochemical performance of the polymers were measured in 1.0 mol·L^{-1} H_2SO_4 solution. Details regarding the specific capacitance calculations were described in the Supplementary information part.

3 Results and discussion

Figure 1(a) shows the preparation process of SWCNT/RuO_2/PIn nanocomposite. The RuO_2 nanoparticles were firstly interact with richly –COOH groups of acid-treated SWCNT, and then PIn layers were coated on the surface of

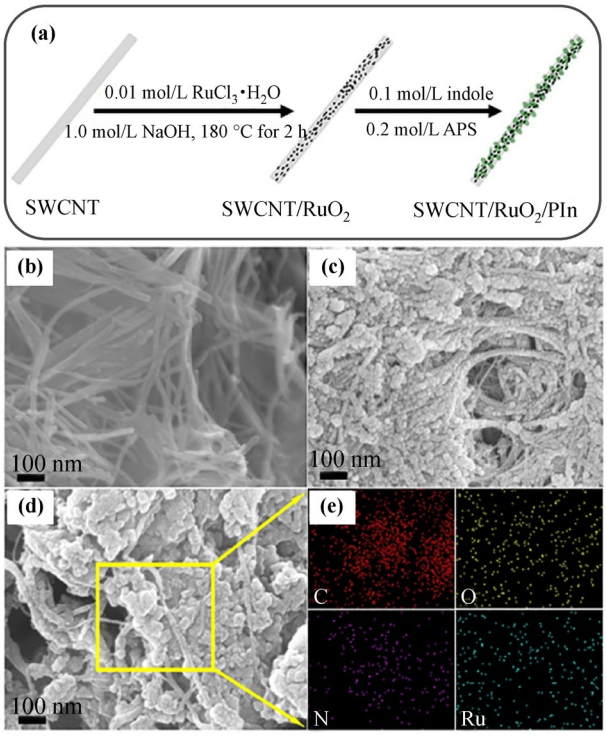

Fig. 1 **(a)** The preparation process of SWCNT/RuO_2/PIn nanocomposite. SEM images of **(b)** SWCNT/PIn, **(c)** SWCNT/RuO_2 and **(d)** SWCNT/RuO_2/PIn samples. **(e)** Elemental mapping images of SWCNT/RuO_2/PIn.

SWCNT/RuO_2. From SEM images, SWCNT/PIn, SWCNT/RuO_2 and SWCNT/RuO_2/PIn all showed nanocable structure. As shown in Fig. 1(b), PIn was covered on the surface of SWCNT. In Fig. 1(c), as-prepared RuO_2 nanoparticles were uniform distribution on the surface of SWCNT. For the SWCNT/RuO_2/PIn nanocomposite (Fig. 1(d)), obviously, PIn was coated on the surface of SWCNT/RuO_2. In addition, the formation of the SWCNT/RuO_2/PIn nanocomposite was also confirmed by C, N, O and Ru elements mapping images (Fig. 1(e)), and their mass percentages were 67.48%, 18.32%, 10.58% and 3.62%, respectively (Fig. S1).

In order to better observe the structure of samples, TEM were carried out. Figure 2 shows TEM images of SWCNT, SWCNT/PIn, SWCNT/RuO_2 and SWCNT/RuO_2/PIn. By comparison of Figs. 2(a) and 2(b), PIn was clearly evident on the surface of SWCNT. Figure 2(c) clearly shows that RuO_2 nanoparticles were distributed over the SWCNT surface. The size of RuO_2 nanoparticles on SWCNT was between 0.5 and 2.5 nm. Without the presence of SWCNT, RuO_2 was easily agglomerated [28]. The result observed from Fig. 2(c) suggested that the functional group on SWCNT had a very important function in the formation

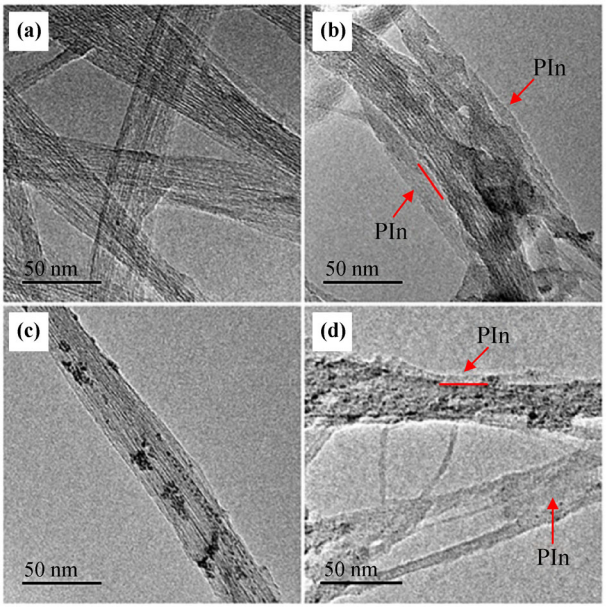

Fig. 2 TEM images of **(a)** SWCNT, **(b)** SWCNT/PIn, **(c)** SWCNT/RuO_2 and **(d)** SWCNT/RuO_2/PIn.

and dispersion of RuO_2 nanoparticles. It was distinctly seen that PIn was coated on the prefabricated SWCNT/RuO_2 binary nanocomposite (Fig. 2(d)), thus forming SWCNT/RuO_2/PIn ternary nanocomposite.

Figure 3(a) shows XRD patterns of PIn, SWCNT/RuO_2, SWCNT/PIn and SWCNT/RuO_2/PIn samples. The XRD pattern of RuO_2 showed broad diffraction peaks at 35.1° and 54.3° (Fig. 3(a), inset), which was indexed to (1 0 1) and (2 1 1) reflections of rutile RuO_2 (JCPDS card No. 43-1027, Fig. S2). The main peaks in the XRD pattern of SWCNT/RuO_2 were located at 24°, 38°, 44°, 58° and 69°, which came from those of SWCNT and RuO_2. As for SWCNT/PIn and SWCNT/RuO_2/PIn nanocomposites, the obvious peaks at 8°, 20° and 26° belonged to PIn. However, the peaks of SWCNT and RuO_2 changed very weak and even disappeared due to the presence of PIn on the surface of SWCNT/RuO_2 nanocomposite. Figure 3(b) presents FTIR spectra of SWCNT, RuO_2, SWCNT/PIn, SWCNT/RuO_2 and SWCNT/RuO_2/PIn. The weak peak at 1625 cm^{-1} was indicative of the –COOH functional group on SWCNT [35]. The vibrational peak at 611 cm^{-1} of rutile RuO_2 was present in the every nanocomposite [36]. At 1573, 1456, 1384, 1110 and 744 cm^{-1}, the spectra of SWCNT/RuO_2/PIn displayed similar peaks as PIn, which corresponded to –N–H, –C=C, –C–N, –C–C and –C–H vibrations [37], respectively. The SWCNT/RuO_2/PIn nanocomposite included the XPS information of each component (Fig. 3(c)), further indicating that this ternary

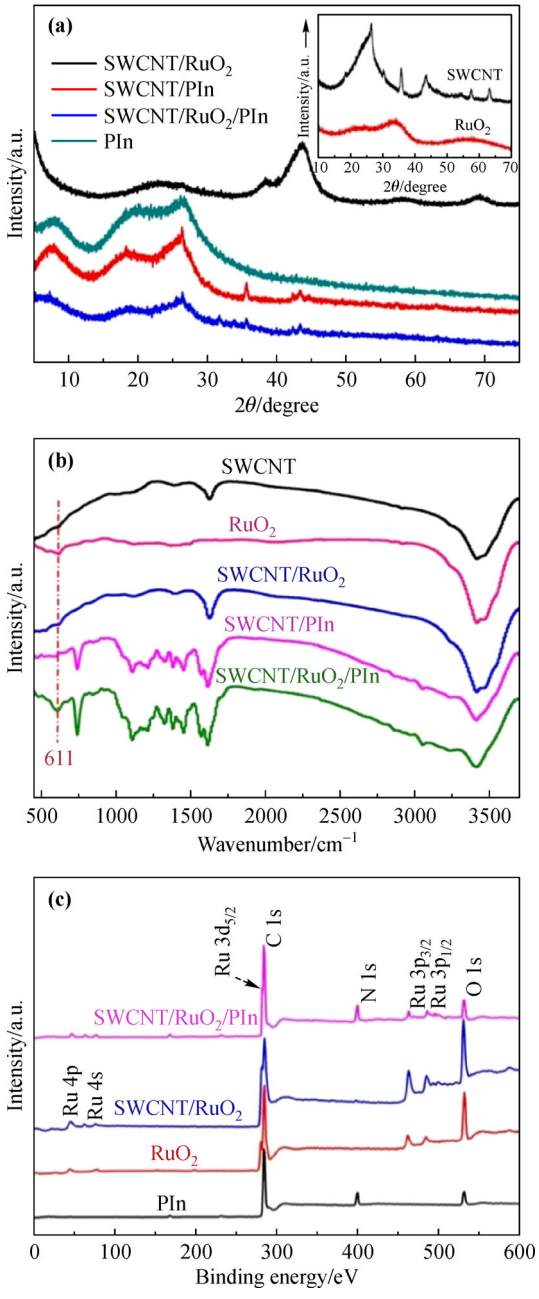

Fig. 3 **(a)** XRD, **(b)** FTIR and **(c)** XPS spectra of SWCNT, RuO_2, SWCNT/RuO_2, SWCNT/PIn and SWCNT/RuO_2/PIn samples.

nanocomposite was composed of SWCNT, RuO_2 and PIn. Namely, the peak at around 400 eV was ascribed to the N 1s signal on PIn. The characteristics of Ru $3d_{5/2}$, Ru $3p_{3/2}$ and Ru $3p_{1/2}$ were observed at 281.5, 462.5 and 484.3 eV [32], respectively, and the peaks at 284.2 and 531.5 eV were attributed to C 1s and O 1s chemical states, respectively, which mainly came from SWCNT and RuO_2.

Figure 4 displays capacitive behaviors of SWCNT/PIn, SWCNT/RuO_2 and SWCNT/RuO_2/PIn electrodes. The

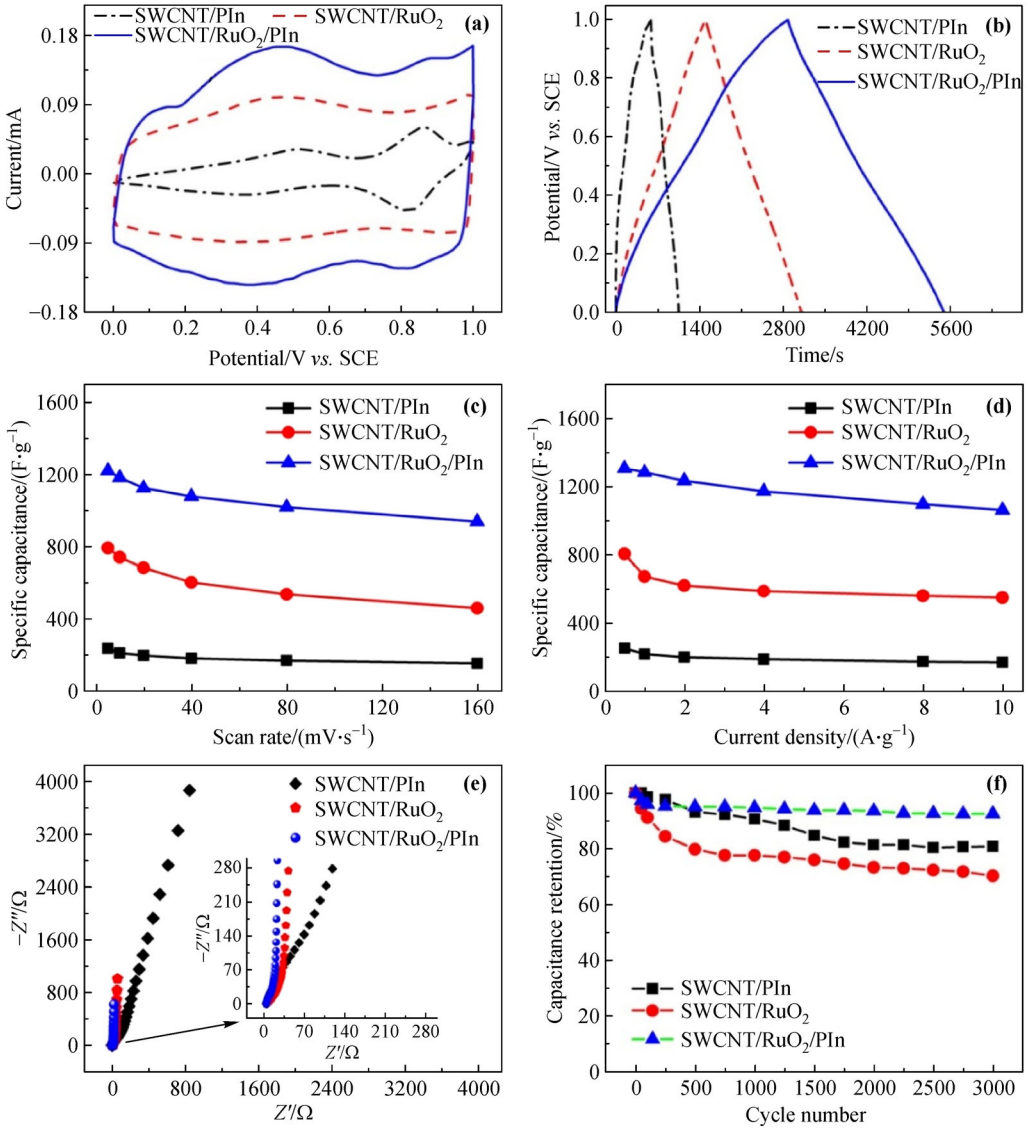

Fig. 4 Electrochemical performance of SWCNT/PIn, SWCNT/RuO_2 and SWCNT/RuO_2/PIn electrodes: **(a)** CV at 5 $mV \cdot s^{-1}$; **(b)** GCD at 0.5 $A \cdot g^{-1}$; **(c)** the relationship between specific capacitance and scan rate; **(d)** the relationship between specific capacitance and current densities; **(e)** Nyquist plots; **(f)** cycle life.

integral area of the cyclic voltammetry (CV) curve for SWCNT/RuO_2 was larger than that for SWCNT/PIn (Fig. 4 (a)), which was due to that RuO_2 had better electrochemical activity compared to PIn (Fig. S3). Moreover, it was seen from Fig. S3 that the CV shapes were different between binary composites and individual components. For example, the current intensity of redox peaks at about 0.8 V was larger than that at about 0.4 V for SWCNT/PIn while a contrary phenomenon was observed for PIn. For SWCNT/RuO_2, the position of redox peaks shifted negatively from 0.6 to 0.4 V relative to RuO_2. The results implied that the combination produced synergistic effect. For the ternary composite, SWCNT/RuO_2/PIn showed the largest CV area, indicative of its high specific capacitance. Furthermore, from the redox peaks (Figs. 4(a) and S3), SWCNT/RuO_2/PIn contained properties of each component, further demonstrating the formation of the composite. Similarly, in the galvanostatic charge–discharge measurement (GCD) curves, SWCNT/RuO_2/PIn also showed a longer discharge time compared to SWCNT/PIn and SWCNT/RuO_2 (Fig. 4 (b)). In Fig. 4(c), SWCNT/RuO_2/PIn exhibited an enhanced specific capacitance of 1222 $F \cdot g^{-1}$ at 5 $mV \cdot s^{-1}$ as compared to those of SWCNT/RuO_2 (793 $F \cdot g^{-1}$) and SWCNT/PIn (237 $F \cdot g^{-1}$), which was superior to 435 $F \cdot g^{-1}$ of RuO_2 and 89 $F \cdot g^{-1}$ of PIn. At 0.5 $A \cdot g^{-1}$, the specific capacitance of SWCNT/RuO_2/PIn reached 1307 $F \cdot g^{-1}$ in

contrast to 805 $F \cdot g^{-1}$ of SWCNT/RuO_2 and 252 $F \cdot g^{-1}$ of SWCNT/PIn (Fig. 4(d)). With increasing the scan rate or current density, the diffusion of ions was difficult to fully access the interior surfaces of the electrode materials, thus leading to the decrease in the specific capacitance [14]. It was particularly gratifying to note that the specific capacitances of SWCNT/RuO_2/PIn decreased slowly with increasing of current densities from 0.5 to 10 $A \cdot g^{-1}$, with a retention of 81%. The value was higher than 69% of SWCNT/RuO_2 and 67% of SWCNT/PIn. The high capacitance and good rate capability of SWCNT/RuO_2/PIn were attributable to the following reasons: 1) The strong interactions such as bond formation between carboxyl groups on SWCNT observed by FTIR and hydroxyl groups of RuO_2 nanoparticles effectively prevented the agglomeration of RuO_2 nanoparticles, and the heterostructure formed direct delivery paths for protons to access the inside of RuO_2, which enhanced the capacitance of the composite [38–39]. 2) RuO_2 and PIn have reversible redox process and large pseudocapacitance in acidic aqueous solution. For example, the theoretical specific capacitance of RuO_2 can reach 1200–2200 $F \cdot g^{-1}$ [40], whereas their actual specific capacitances were lower possibly because of the low conductivity [18,28]. SWCNT not only serves as the support for the dispersion of RuO_2 nanoparticles and the PIn film, but more importantly, also provides straight conducting pathways for electrons, thus greatly promoting the specific capacitance enhancement of the composite. 3) Both RuO_2 and PIn emerge good pseudocapacitive behaviours in H_2SO_4 solution by their redox reactions as shown in Scheme 1, respectively. The simultaneously electrochemical active in the H_2SO_4 system is instrumental in enhancing the capacitance of the SWCNT/RuO_2/PIn composite.

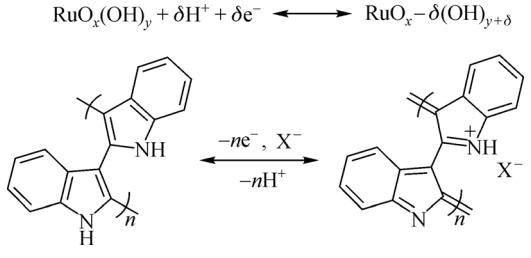

Scheme 1 Reaction mechanisms of RuO_2 and PIn electrodes in H_2SO_4 solution, respectively.

Electrochemical impedance spectroscopy (EIS) results were measured from 0.01 Hz to 100 kHz. Figure 4(e) shows Nyquist plots of SWCNT/PIn, SWCNT/RuO_2 and SWCNT/RuO_2/PIn electrodes. The diameter of arc in high frequency represents the charge transfer resistance (R_{ct}), and the intercept on the real axis corresponds to the ohmic resistance. All electrodes had almost equal ohmic resistance value of about 5 Ω, indicating the same electrolyte used for all the electrochemical measurements. It was measured from the diameter of arc that the SWCNT/RuO_2/PIn electrode had a smaller R_{ct} value (9 Ω) compared with SWCNT/RuO_2 (21 Ω), SWCNT/PIn (37 Ω) and SWCNT (71 Ω) (Fig. S4). This indicated the RuO_2/PIn coating had a cooperation effect between RuO_2 and PIn. In the low-frequency range, the slope of the 45° portion is defined as the Warburg resistance (R_w), corresponding to ion diffusion to the electrode interface [41]. The R_w value of SWCNT/RuO_2/PIn was larger than those of SWCNT/RuO_2 and SWCNT/PIn electrodes. This indicated a good accessibility of ions to the SWCNT/RuO_2/PIn electrode. In addition, the SWCNT/RuO_2/PIn electrode exhibited a more vertical line in the low-frequency range than the other two, revealing an ideal capacitive behavior. According to $C = 1/(2\pi fZ'')$, the calculated specific capacitance of SWCNT/RuO_2/PIn at 0.01 Hz was 1282 $F \cdot g^{-1}$, superior to those of SWCNT/RuO_2 (784 $F \cdot g^{-1}$) and SWCNT/PIn (206 $F \cdot g^{-1}$). This indicated that the SWCNT/RuO_2/PIn electrode had a good capacitive performance.

The cycling life is a very significant parameter for electrode materials. Here, the nano-coating of PIn enormously boosted the cycling stability at a relatively large current density of 30 $A \cdot g^{-1}$. For example, the SWCNT/RuO_2/PIn electrode showed 93% retention rate after 3000 cycles (Fig. 4(f)), higher than those of SWCNT/PIn (81%) and SWCNT/RuO_2 (70%) electrodes. This result indicated that the nano-coating of PIn with high electrochemical and mechanical stabilities prevented RuO_2 nanoparticles from structural changing and breaking during the repeated cycling [18]. Furthermore, the specific capacitance and cycling life of SWCNT/RuO_2/PIn were compared with other reported materials as listed in Table 1 [14–16,20,25,33,42–49]. Clearly, SWCNT/RuO_2/PIn has preferable capacitive performance.

The ternary SWCNT/RuO_2/PIn nanocomposite was also used to assemble symmetric supercapacitor and characterized by CV and GCD methods. In Fig. 5(a), the CV curves had a large integral area, indicative of high capacitance. Correspondingly, GCD curves were symmetric triangular shape at different current densities (Fig. 5(b)), the specific capacitance decreased from 1203, 1148, 1092, 969 to 936 $F \cdot g^{-1}$ when the discharge current density was increased from

Table 1 Capacitance and cycling life comparison of SWCNT/RuO_2/PIn with some important composites materials [14–16,20,25,33,42–49]

Ternary composite	Specific capacitance	Capacitance retention	Refs.
MnO_2/PPy/CNF	705 $F\cdot g^{-1}$ at 2 $mV\cdot s^{-1}$	91% after 2000 cycles at 12 $mA\cdot cm^{-2}$	[14]
CNT@PPy@MnO_2	325 $F\cdot g^{-1}$ at 2 $mV\cdot s^{-1}$	90.2% after 1000 cycles at 100 $mV\cdot s^{-1}$	[15]
CNT/PAN/MnO_2	330 $F\cdot g^{-1}$ at 5 $mV\cdot s^{-1}$	77% after 1000 cycles at 20 $mV\cdot s^{-1}$	[16]
PIn/CNT	555 $F\cdot g^{-1}$ at 1.0 $A\cdot g^{-1}$	96.9% after 2000 cycles at 20 $mV\cdot s^{-1}$	[20]
V_2O_5/PIn/carbon cloth	535.3 $F\cdot g^{-1}$ at 1.0 $A\cdot g^{-1}$	91% after 5000 cycles at 10 $A\cdot g^{-1}$	[25]
RGO/RuO_2/PEDOT	184 $F\cdot g^{-1}$ at 1 $mV\cdot s^{-1}$	70% after 5000 cycles at 1 $A\cdot g^{-1}$	[42]
GE–SnO_2–PAN	913.4 $F\cdot g^{-1}$ at 5 $mV\cdot s^{-1}$	90.8% after 1000 cycles at 1.2 $A\cdot g^{-1}$	[43]
PPy/RGO/Fe_2O_3	125.7 $F\cdot g^{-1}$ at 0.5 $A\cdot g^{-1}$	81.3% after 200 cycles at 0.5 $A\cdot g^{-1}$	[44]
MnO_2/rGO/PEDOT:PSS	169.1 $F\cdot g^{-1}$ at 0.2 $A\cdot g^{-1}$	66.2% after 2000 cycles at 10 $A\cdot g^{-1}$	[45]
SG/MnO_2/PAN	276 $F\cdot g^{-1}$ at 1 $A\cdot g^{-1}$	88.3% after 3000 cycles at 1 $A\cdot g^{-1}$	[46]
PAN–MWNTs–TiO_2	525 $F\cdot g^{-1}$ at 1 $mV\cdot s^{-1}$	67% after 6000 cycles at 4 $A\cdot g^{-1}$	[47]
RGO/RuO_2	357 $F\cdot g^{-1}$ at 0.3 $A\cdot g^{-1}$	70% after 2500 cyclesat 16 $A\cdot g^{-1}$	[48]
RuO_2 networks	628 $F\cdot g^{-1}$ at 0.5 $A\cdot g^{-1}$	86% after 4000 cycles at 5.0 $A\cdot g^{-1}$	[49]
RuO_2/PEDOT:PSS/GE	820 F g^{-1} at 0.5 $A\cdot g^{-1}$	81.5% after 1000 cycles at 0.5 $A\cdot g^{-1}$	[33]
SWCNT/RuO_2/PIn	1307 $F\cdot g^{-1}$ at 0.5 $A\cdot g^{-1}$	93% after 3000 cycles at 30 $A\cdot g^{-1}$	this work

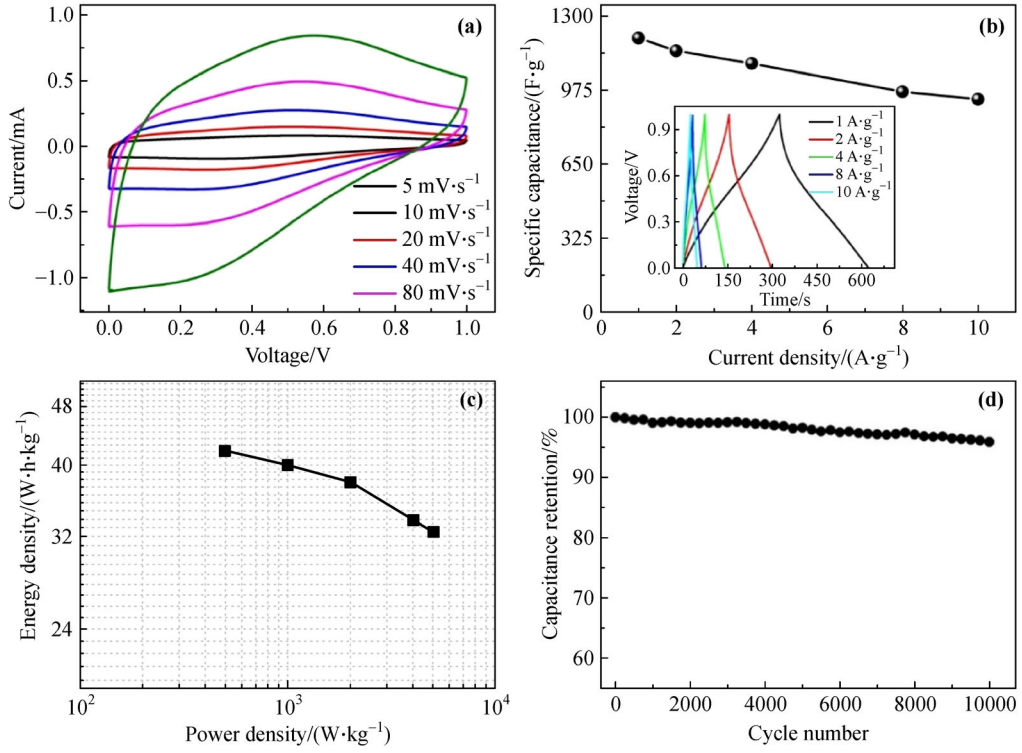

Fig. 5 Electrochemical performance of the supercapacitor based on SWCNT/RuO_2/PIn: **(a)** CV at different scan rates; **(b)** specific capacitance as a function of current density (inset: GCD at different current densities); **(c)** Ragone plots of supercapacitor in comparison with the values reported for other devices; **(d)** cycle life at 10 $A\cdot g^{-1}$.

1, 2, 4, 8 and 10 $A\cdot g^{-1}$, and the capacitance retention reached 78%. These values highlighted that the supercapacitor based on SWCNT/RuO_2/PIn nanocomposites possessed high specific capacitance and good rate capability.

The Ragone plot of symmetric device based on SWCNT/RuO_2/PIn electrodes has been made, as shown in Fig. 5(c). The energy density of 42 $W\cdot h\cdot kg^{-1}$ was obtained at 500 $W\cdot kg^{-1}$, which still remained a high value of 33 $W\cdot h\cdot kg^{-1}$ when the power density was 5000 $W\cdot kg^{-1}$. The energy

density decreased very slowly with increasing of the power density, and the corresponding energy densities were higher than those in some latest papers that employed RuO_2/GE-based devices such as RuO_2/GE/CNT (39.28 W·h·kg^{-1} at 356 W·kg^{-1}, 33.38 W·h·kg^{-1} at 4500 W·kg^{-1}) [32], RGO/RuO_2 (22.7 W·h·kg^{-1} at 124 W·kg^{-1}, 10 W·h·kg^{-1} at 4000 W·kg^{-1}) [48], and RuO_2/GE (20.1 W·h·kg^{-1} at 50 W·kg^{-1}, 7.0 W·h·kg^{-1} at 5000 W·kg^{-1}) [31]. The excellent performance of the as-fabricated supercapacitor based on SWCNT/RuO_2/PIn could be ascribed to the following reasons: 1) ultrafine RuO_2 nanoparticles (about 1.2 nm) were beneficial to maximize the specific capacitance by itself; 2) SWCNT enhanced the conductivity of nanocomposites, thus accelerating the electrons/charges transport; 3) PIn with pseudocapacitive behaviors on the one hand contributed to specific capacitance, on the other hand, made the binder-free electrode have a low internal resistance.

The cycling life was measured at 10 A·g^{-1}. As shown in Fig. 5(d), the capacitance loss after 10000 cycles was negligible, at about 5% loss. The 95% retention of initial capacitance indicated that the supercapacitor based on SWCNT/RuO_2/PIn had long-term electrochemical stability. The excellent stability may be attributed to the fact that the outmost PIn layer was helpful for the improvement of the stability of ultrafine RuO_2 nanoparticles by the protective functions of PIn with high electrochemical stability.

4 Conclusions

The ternary SWCNT/RuO_2/PIn nanocomposite was prepared and its capacitive behaviors were valuated. The specific capacitance of SWCNT/RuO_2/PIn reached 1283 F·g^{-1} at 1.0 A·g^{-1}, and the symmetric supercapacitor based on SWCNT/RuO_2/PIn electrodes also showed good cycling stability, superior capacitive performance of 1203 F·g^{-1} at 1.0 A·g^{-1} and high energy density of 42 W·h·kg^{-1} at 500 W·kg^{-1}, while the energy density still remained a high value of 33 W·h·kg^{-1} even at 5000 W·kg^{-1}. The excellent performance makes the ternary SWCNT/RuO_2/PIn nanocomposite attractive for the application in supercapacitors.

Acknowledgements This work was supported by the National Natural Science Foundation of China (Grant Nos. 51862011 and 51662012), the Jiangxi Outstanding Young Talent Fund Projects (20171BCB23076), the Natural Science Foundation of Jiangxi Province (20171BAB206013), and the Young Top-Notch Talent of Jiangxi Science and Technology Normal University (2016QNBJRC001).

References

[1] Zhang L L, Zhao X S. Carbon-based materials as supercapacitor electrodes. Chemical Society Reviews, 2009, 38(9): 2520–2531

[2] Simon P, Gogotsi Y. Materials for electrochemical capacitors. Nature Materials, 2008, 7(11): 845–854

[3] Sellam, Hashmi S A. High rate performance of flexible pseudocapacitors fabricated using ionic-liquid-based proton conducting polymer electrolyte with poly(3, 4-ethylenedioxythiophene):poly(styrene sulfonate) and its hydrous ruthenium oxide composite electrodes. ACS Applied Materials & Interfaces, 2013, 5(9): 3875–3883

[4] Liang A Q, Li D Q, Zhou W Q, et al. Robust flexible WS_2/PEDOT:PSS film for use in high-performance miniature supercapacitors. Journal of Electroanalytical Chemistry, 2018, 824: 136–146

[5] Zhang L, Gu H, Sun H, et al. Molecular level one-step activation of agar to activated carbon for high performance supercapacitors. Carbon, 2018, 132: 573–579

[6] Kumar Y, Pandey G P, Hashmi S A. Gel polymer electrolyte based electrical double layer capacitors: comparative study with multiwalled carbon nanotubes and activated carbon electrodes. The Journal of Physical Chemistry C, 2012, 116(50): 26118–26127

[7] Barranco V, Lillo-Rodenas M A, Linares-Solano A, et al. Amorphous carbon nanofibers and their activated carbon nanofibers as supercapacitor electrodes. The Journal of Physical Chemistry C, 2010, 114(22): 10302–10307

[8] Stoller M D, Park S, Zhu Y, et al. Graphene-based ultracapacitors. Nano Letters, 2008, 8(10): 3498–3502

[9] Biswas S, Drzal L T. Multilayered nano-architecture of variable sized graphene nanosheets for enhanced supercapacitor electrode performance. ACS Applied Materials & Interfaces, 2010, 2(8): 2293–2300

[10] Zhou W Q, Ma X M, Jiang F X, et al. Electrochemical fabrication of a porous network MnO_2/poly(5-cyanoindole) composite and its capacitance performance. Electrochimica Acta, 2014, 138: 270–277

[11] Wang G, Zhang L, Zhang J. A review of electrode materials for electrochemical supercapacitors. Chemical Society Reviews, 2012, 41(2): 797–828

[12] Hou Y, Cheng Y, Hobson T, et al. Design and synthesis of hierarchical MnO_2 nanospheres/carbon nanotubes/conducting polymer ternary composite for high performance electrochemical electrodes. Nano Letters, 2010, 10(7): 2727–2733

[13] Lv P, Feng Y Y, Li Y, et al. Carbon fabric-aligned carbon nanotube/MnO_2/conducting polymers ternary composite electrodes with high utilization and mass loading of MnO_2 for supercapacitors. Journal of Power Sources, 2012, 220: 160–168

[14] Wang J G, Yang Y, Huang Z H, et al. Rational synthesis of MnO_2/conducting polypyrrole@carbon nanofiber triaxial nano-cables for high-performance supercapacitors. Journal of Materials Chemistry, 2012, 22(33): 16943–16949

[15] Li P, Yang Y, Shi E, et al. Core–double-shell, carbon nanotube@polypyrrole@MnO_2 sponge as freestanding, compressible supercapacitor electrode. ACS Applied Materials & Interfaces, 2014, 6(7): 5228–5234

[16] Li Q, Liu J, Zou J, et al. Synthesis and electrochemical performance of multi-walled carbon nanotube/polyaniline/MnO_2 ternary coaxial nanostructures for supercapacitors. Journal of Power Sources, 2011, 196(1): 565–572

[17] Zhou W Q, Xu J K. Progress in conjugated polyindoles: synthesis, polymerization mechanisms, properties, and applications. Polymer Reviews, 2017, 57(2): 248–275

[18] Zhou Q J, Zhu D H, Ma X M, et al. High-performance capacitive behavior of layered reduced graphene oxide and polyindole nanocomposite materials. RSC Advances, 2016, 6(35): 29840–29847

[19] Zhang F, Yuan C, Zhu J, et al. Flexible films derived from electrospun carbon nanofibers incorporated with Co_3O_4 hollow nanoparticles as self-supported electrodes for electrochemical capacitors. Advanced Functional Materials, 2013, 23(31): 3909–3915

[20] Tebyetekerwa M, Wang X, Wu Y, et al. Controlled synergistic strategy to fabricate 3D-skeletal hetero-nanosponges with high performance for flexible energy storage applications. Journal of Materials Chemistry A: Materials for Energy and Sustainability, 2017, 5(40): 21114–21121

[21] Tebyetekerwa M, Yang S, Peng S, et al. Unveiling polyindole: freestanding as-electrospun polyindole nanofibers and polyindole/carbon nanotubes composites as enhanced electrodes for flexible all-solid-state supercapacitors. Electrochimica Acta, 2017, 247: 400–409

[22] Wang W, Wu S. A new ternary composite based on carbon nanotubes/polyindole/graphene with preeminent electrocapacitive performance for supercapacitors. Applied Surface Science, 2017, 396: 1360–1367

[23] Zhou Q, Zhu D, Ma X, et al. PEDOT:PSS-assisted polyindole hollow nanospheres modified carbon cloth as high performance electrochemical capacitor electrodes. Electrochimica Acta, 2016, 212: 662–670

[24] Majumder M, Choudhary R B, Koiry S P, et al. Gravimetric and volumetric capacitive performance of polyindole/carbon black/MoS_2 hybrid electrode material for supercapacitor applications. Electrochimica Acta, 2017, 248: 98–111

[25] Zhou X, Chen Q, Wang A, et al. Bamboo-like composites of V_2O_5/polyindole and activated carbon cloth as electrodes for all-solid-state flexible asymmetric supercapacitors. ACS Applied Materials & Interfaces, 2016, 8(6): 3776–3783

[26] Zhou X, Wang A Q, Pan Y M, et al. Facile synthesis of a Co_3O_4@carbon nanotubes/polyindole composite and its application in all-solid-state flexible supercapacitors. Journal of Materials Chemistry A: Materials for Energy and Sustainability, 2015, 3 (24): 13011–13015

[27] Raj R P, Ragupathy P, Mohan S. Remarkable capacitive behavior of a Co_3O_4–polyindole composite as electrode material for supercapacitor applications. Journal of Materials Chemistry A: Materials for Energy and Sustainability, 2015, 3(48): 24338–24348

[28] Chang Y N, Zhou W Q, Wu J, et al. High-performance flexible-film supercapacitors of layered hydrous RuO_2/poly(3,4-ethylenedioxythiophene)-poly(styrenesulfonate) through vacuum filtration. Electrochimica Acta, 2018, 283: 744–754

[29] Deshmukh P R, Bulakhe R N, Pusawale S N, et al. Polyaniline–RuO_2 composite for high performance supercapacitors: chemical synthesis and properties. RSC Advances, 2015, 5(36): 28687–28695

[30] Zheng W, Cheng Q M, Wang D W, et al. High-performance solid-state on-chip supercapacitors based on Si nanowires coated with ruthenium oxide via atomic layer deposition. Journal of Power Sources, 2017, 341: 1–10

[31] Wu Z S, Wang D W, Ren W, et al. Anchoring hydrous RuO_2 on graphene sheets for high-performance electrochemical capacitors. Advanced Functional Materials, 2010, 20(20): 3595–3602

[32] Wang W, Guo S, Lee I, et al. Hydrous ruthenium oxide nanoparticles anchored to graphene and carbon nanotube hybrid foam for supercapacitors. Scientific Reports, 2014, 4(1): 4452

[33] Cho S, Kim M, Jang J. Screen-printable and flexible RuO_2 nanoparticle-decorated PEDOT:PSS/graphene nanocomposite with enhanced electrical and electrochemical performances for high-capacity supercapacitor. ACS Applied Materials & Interfaces, 2015, 7(19): 10213–10227

[34] Yu Z, Tetard L, Zhai L, et al. Supercapacitor electrode materials: nanostructures from 0 to 3 dimensions. Energy & Environmental Science, 2015, 8(3): 702–730

[35] Li C, Chen Y H, Wang Y B, et al. A fullerene–single wall carbon nanotube complex for polymer bulk heterojunction photovoltaic cells. Journal of Materials Chemistry, 2007, 17(23): 2406–2411

[36] Mink J, Kristof J, Battisti A D, et al. Investigation on the formation of RuO_2-based mixed-oxide coatings by spectroscopic methods. Surface Science, 1995, 335(1–3): 252–257

[37] Ma X M, Zhou W Q, Mo D Z, et al. One-step template-free electrodeposition of novel poly (indole-7-carboxylic acid) nanowires and their high capacitance properties. RSC Advances, 2015, 5(5): 3215–3223

[38] Kim Y T, Tadai K, Mitani T. Highly dispersed ruthenium oxide nanoparticles on carboxylated carbon nanotubes for supercapacitor electrode materials. Journal of Materials Chemistry, 2005, 15 (46): 4914–4921

[39] Zhang W D, Xu B, Jiang L C. Functional hybrid materials based on carbon nanotubes and metal oxides. Journal of Materials Chemistry, 2010, 20(31): 6383–6391

[40] Zhi M, Xiang C, Li J, et al. Nanostructured carbon–metal oxide composite electrodes for supercapacitors: a review. Nanoscale, 2013, 5(1): 72–88

[41] Wang K, Meng Q H, Zhang Y J, et al. High-performance two-ply yarn supercapacitors based on carbon nanotubes and polyaniline nanowire arrays. Advanced Materials, 2013, 25(10): 1494–1498

[42] Wang W J, Lei W, Yao T Y, et al. One-pot synthesis of graphene/SnO_2/PEDOT ternary electrode material for supercapacitors. Electrochimica Acta, 2013, 108: 118–126

[43] Jin Y H, Jia M Q. Design and synthesis of nanostructured graphene–SnO_2–polyaniline ternary composite and their excellent supercapacitor performance. Colloids and Surfaces A: Physicochemical and Engineering Aspects, 2015, 464: 17–25

[44] Eeu Y C, Lim H N, Lim Y S, et al. Electrodeposition of polypyrrole/reduced graphene oxide/iron oxide nanocomposite as supercapacitor electrode material. Journal of Nanomaterials, 2013, 2013: 653890 (6 pages)

[45] Yan D, Liu Y, Li Y H, et al. Synthesis and electrochemical properties of MnO_2/rGO/PEDOT:PSS ternary composite electrode material for supercapacitors. Materials Letters, 2014, 127: 53–55

[46] Wang G X, Tang Q Q, Bao H, et al. Synthesis of hierarchical sulfonated graphene/MnO_2/polyaniline ternary composite and its improved electrochemical performance. Journal of Power Sources, 2013, 241: 231–238

[47] Singu B S, Male U, Srinivasan P, et al. Preparation and performance of polyaniline–multiwall carbon nanotubes–titanium dioxide ternary composite electrode material for supercapacitors. Journal of Industrial and Engineering Chemistry, 2017, 49: 82–87

[48] Zhang J T, Jiang J W, Li H L, et al. A high-performance asymmetric supercapacitor fabricated with graphene-based electrodes. Energy & Environmental Science, 2011, 4(10): 4009–4015

[49] Peng Z, Liu X, Meng H, et al. Design and tailoring of the 3D macroporous hydrous RuO_2 hierarchical architectures with a hard-template method for high-performance supercapacitors. ACS Applied Materials & Interfaces, 2017, 9(5): 4577–4586

Supplementary information

The working electrode was prepared by a typical method. The electroactive materials in ethanol solution (10 μL, 2 $mg \cdot mL^{-1}$) were dropped on glass carbon substrates (GC, diameter 3 mm) and dried in vacuum at 45 °C for 30 min, the mass loading was 0.29 $mg \cdot cm^{-2}$. The specific capacitance of the single electrode was calculated from CV and GCD curves measured on the three-electrode configuration or the symmetric supercapacitor according to Eqs. (S1)–(S3) [S1], respectively:

$$C_{s1} = \frac{\int_{E_1}^{E_2} i(E)\mathrm{d}E}{2\nu m(E_2 - E_1)} \tag{S1}$$

$$C_{s2} = \frac{I \times \Delta t_d}{m \times \Delta V} \tag{S2}$$

$$C_{s3} = \frac{4 \times I \times \Delta t_d}{M \times \Delta V} \tag{S3}$$

where, C_{s1}, C_{s2} and C_{s3} are specific capacitance (unit: F $\cdot g^{-1}$); E_1 and E_2 are cutoff potentials in CV; $i(E)$ is the instantaneous current; $\int_{E_1}^{E_2} i(E)\mathrm{d}E$ is the total voltammetric charge obtained by integration in CV; v is the scan rate; I and Δt_d are the discharge current (unit: A) and time (unit: s), respectively; ΔV is the potential range (unit: V); m is the mass of one electrode (unit: g); and M is the total mass of two electrodes (unit: g).

The power density (P, unit: $W \cdot kg^{-1}$) and energy density (E, unit: $W \cdot h \cdot kg^{-1}$) values of the electrode materials were calculated by the following Eqs. (S4) and (S5) [S1]:

$$E = \frac{1}{8} \times \frac{1000}{3600} \times C_{s3} \times \Delta V^2 \tag{S4}$$

$$P = \frac{3600 \times E}{\Delta t_d} \tag{S5}$$

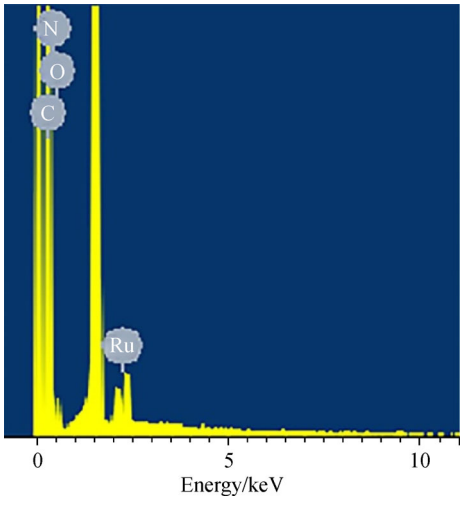

Fig. S1 The energy dispersive spectroscopy (EDS) result of SWCNT/RuO_2/PIn.

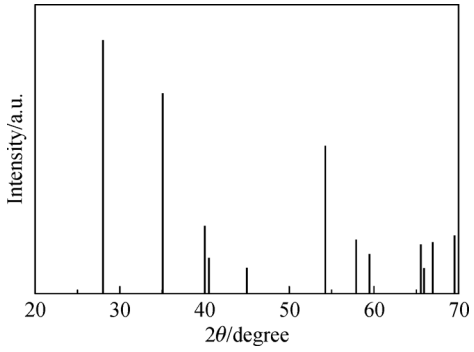

Fig. S2 The XRD pattern of rutile RuO_2 (JCPDS card No. 43-1027).

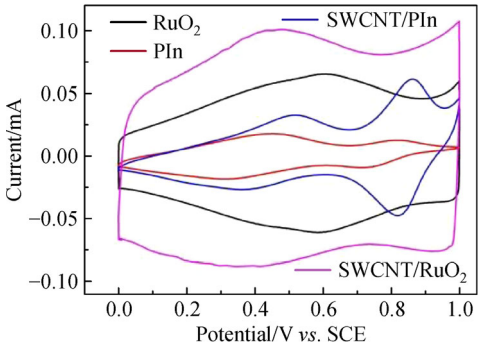

Fig. S3 CV curves of RuO_2, PIn, SWCNT/PIn and SWCNT/RuO_2 electrodes in 1.0 mol·L^{-1} H_2SO_4 solution at 10 mV·s^{-1}.

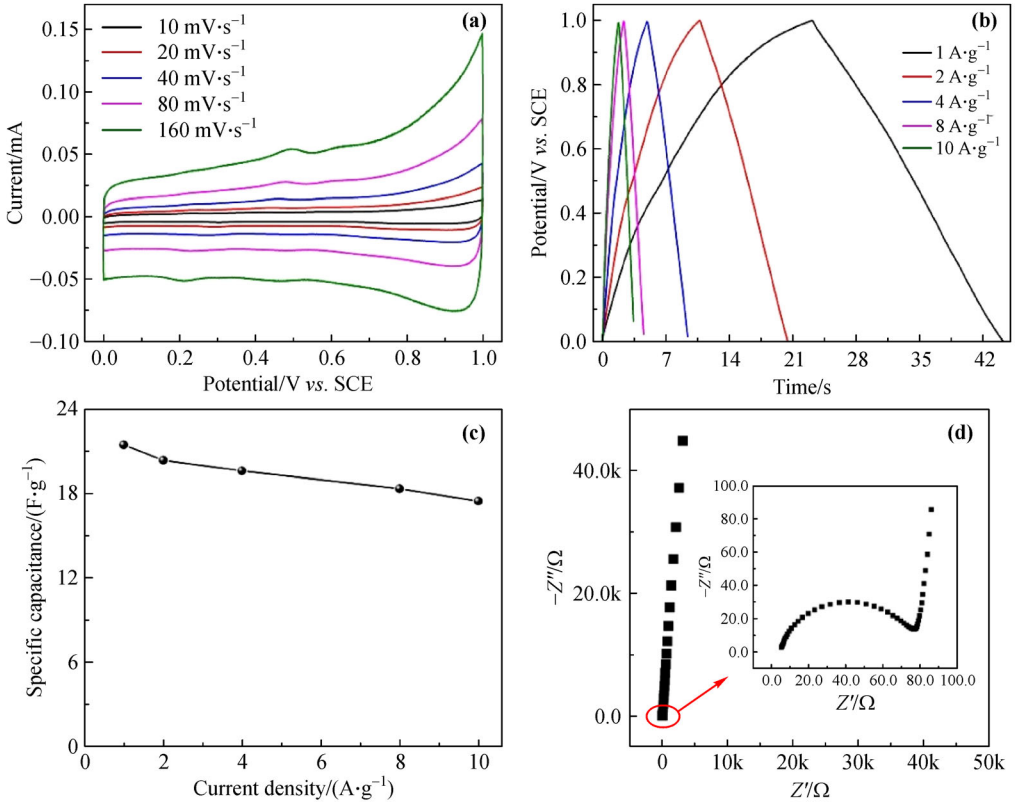

Fig. S4 Electrochemical performance of the SWCNT electrode: **(a)** CV curves at different scan rates; **(b)** GCD at different current densities; **(c)** the relationship between specific capacitance and current density; **(d)** the Nyquist plot.

Reference

[S1] Zhou W Q, Xu J K. High-operating-voltage all-solid-state symmetrical supercapacitors based on poly(3,4-ethylenedioxythiophene)/poly (styrenesulfonate) films treated by organic solvents. Electrochimica Acta, 2016, 222: 1895–1902